# Transformation of nanoscale and ionic Cu and Zn during the incineration of digested sewage sludge (biosolids)

Jonas Wielinski[1,2], Alexander Gogos[1], Andreas Voegelin[1], Christoph Müller[3], Eberhard Morgenroth[1,2], Ralf Kaegi[1,*]

[1] Eawag, Swiss Federal Institute of Aquatic Science and Technology, 8600 Dübendorf, Switzerland

[2] ETH Zürich, Institute of Environmental Engineering, 8093 Zürich, Switzerland

[3] ETH Zürich, Institute of Energy Technology, 8092 Zürich, Switzerland

*Corresponding author: Ralf Kaegi[1], ralf.kaegi@eawag.ch, Eawag, Überlandstrasse 133, 8600 Dübendorf, Switzerland.

This document is the accepted manuscript version of the following article:
Wielinski, J., Gogos, A., Voegelin, A., Müller, C., Morgenroth, E., & Kaegi, R. (2019). Transformation of nanoscale and ionic Cu and Zn during the incineration of digested sewage sludge (Biosolids). Environmental Science and Technology.
https://doi.org/10.1021/acs.est.9b01983

14 **TOC/Abstract art**

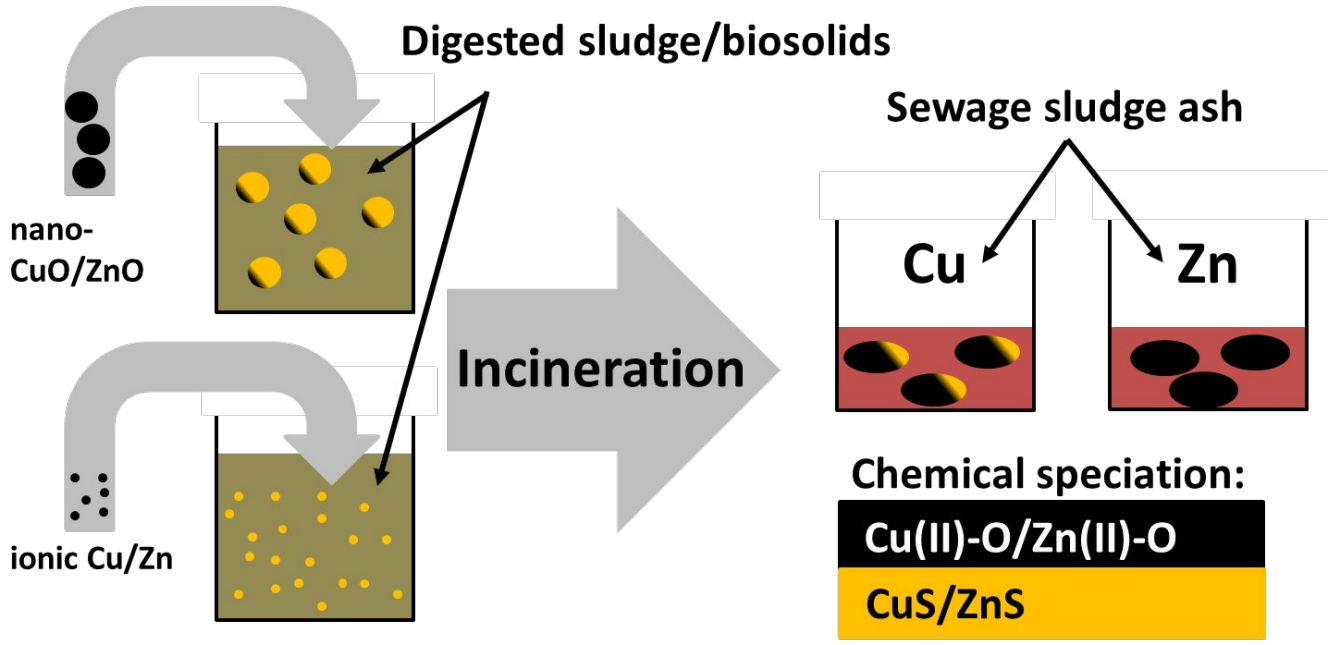


15

16

**Abstract.** Engineered nanoparticles (NP) discharged to sewers are efficiently retained by wastewater treatment plants and accumulate in the sewage sludge, which is commonly digested. The resulting biosolids are either used as fertilizer or incinerated. In this study, we address the transformation of Cu and Zn during sewage sludge incineration and evaluate whether the form of Cu or Zn (nanoparticulate versus dissolved) added to the digested sewage sludge affects the fate of the metals during incineration. We spiked CuO-NP, dissolved $CuSO_4$, ZnO-NP or dissolved $ZnSO_4$ to anaerobically digested sewage sludge to reach Cu and Zn concentrations of ≈°2500°mg/kg and ≈°3700°mg/kg and maintained the sludge under mesophilic, anaerobic conditions for 24 h. Subsequently, the sludge was incinerated in a pilot fluidized bed reactor. The speciation of Cu and Zn in the sludge, derived from X-ray absorption spectroscopy measurements, was dominated by sulfidic species, with > 90% of Cu and > 60% of Zn coordinated to reduced sulfur groups. In the ash, both Cu (> 60%) and Zn (~100%) were coordinated to oxygen. The chemical speciation of Cu and Zn in the ashes was independent of whether they were spiked in dissolved or nanoparticulate form and closely matched the speciation of Cu and Zn observed in ashes from field-scale incinerators.

**Keywords**: Sewage sludge, biosolids, incineration, CuO, ZnO, nanoparticle, transformation

# 1 Introduction

A major share of engineered nanoparticles (ENPs) applied in industrial processes and consumer products is discharged to sewer systems and transported to wastewater treatment plants (WWTPs) after the use phase.[1-2] In general, WWTPs effectively remove over 95% of the incoming ENPs from the wastewater stream, resulting in their accumulation in the sewage sludge.[2-4] The European Commission (EC) Directive 91/271/EEC lowered the maximum amount of C, N and P that can be discharged into surface waters through WWTPs, which led to an increased sewage sludge production in Europe.[5-6] For stabilization, volume reduction, odor removal and energy production, a mixture of primary and excess activated sludge is commonly digested anaerobically.[7] The sludge (or biosolids), resulting from anaerobic digestion, is applied in agriculture (55%), incinerated (25%), composted (10%) or landfilled (8%) in the EU.[6, 8-9] In the

USA, about 25% of the biosolids are incinerated, and in Japan the share of biosolids incineration reaches about 50%.[10] In mono-incineration facilities the sludge is the only target fuel. To start the incineration and for process control, auxiliary fuels such as gas or oil are used. In the co-incineration, sludge is combusted together with other fuels, e.g. coal or municipal solid waste.[10] Mono-incineration is, therefore, very promising as it significantly reduces the sludge volume, destroys harmful organic compounds such as pathogens or organic micro-pollutants, and microplastic and additionally offers the possibility to recover phosphorus from the ash at a later stage.[10] In Switzerland, digested sludge is preferably incinerated in mono-incineration fluidized bed reactors and the resulting ash is landfilled for resource recovery in the future.[11-12]

Cu and Zn are trace elements in the sewage sludge with concentrations ranging from 200 to 1000 mg/kg total suspended solids, respectively.[13] The main sources of Cu and Zn and CuO and ZnO-nanoparticles (NP) in wastewater are the electroplating and metal finishing industries [14] as well as personal care products, paints and (food) packaging materials [1, 15-16]. As previously pointed out, major loads of ENP from such applications will end up in the biosolids with following incineration becoming increasingly important in the future.[6, 17] A recent X-ray absorption spectroscopy (XAS) study suggested that Cu is either bound to sulphur, humic acid or phosphate in fresh and aged biosolids. Zn was bound to either phosphate, reduced sulfur from sulfhydryl groups (e.g cysteine) or substituted in ferrihydrite.[18] A comparable study suggested that ZnO-NP dissolve and mainly re-precipitate as Zn sulfide during sewage sludge digestion.[19] However, the change of the chemical speciation of the Cu and Zn during the incineration process has not been addressed to date, and was therefore the focus of this work. CuO-NP, dissolved $CuSO_4$, ZnO-NP and dissolved $ZnSO_4$ were spiked to separate batches of a municipal, digested sewage sludge, reacted under mesophilic, anaerobic conditions for 24 hours and subsequently incinerated in a pilot bubbling bed type fluidized bed reactor (FBR). XAS was used to assess the chemical speciation of Cu/Zn in the sludge and in the resulting ash. To ensure that experimental conditions in the pilot FBR resulted in chemical Cu/Zn speciation in the ash comparable to the Cu/Zn speciation found in ash from field-scale reactors, sludge and ash samples were additionally collected from three different WWTPs with

onsite FBR and the sludge was also incinerated in our pilot FBR. The chemical speciation of Cu/Zn of the two ashes (field scale and pilot FBR) was compared based on XAS data.

# 2 Materials and methods

## 2.1 Pilot fluidized bed reactor (FBR)

A bubbling bed type pilot FBR was set up to mimic the incineration of sewage sludge in full scale reactors. Briefly, a 10 cm diameter sand bed was kept under conventional fluidization conditions between 820 and 840 °C. The fly ash was collected by two electrostatic precipitators and a filter bag. The dried sludge was continuously fed into the sand bed by a spiral conveyer. The incineration capacity was between 0.8 and 1 kg sludge per hour. Depending on the fuel load in the bed, the residual oxygen content in the flue gas was between 12 and 16%. A detailed description of the pilot reactor is given in SI (Section S1).

## 2.2 Analytical techniques, digestion protocols and chemicals

$CuSO_4$, $ZnSO_4$, $H_2O_2$ (30%), were purchased from Sigma-Aldrich (Switzerland). Suprapure $HNO_3$ (69%) was obtained from Roth (The Netherlands). Suprapure HCl (37%) and Suprapure HF (40%) were purchased from Merck (Germany). All chemicals were used as received. Digestions of sewage sludge were performed with 10 to 20 mg of dried sample and using $H_2O_2$ (2 mL), aqua regia (9 mL) and a microwave (ETHOS 1, MLS, Germany). Digestions of sewage sludge ash were performed with 10 to 20 mg of dried sample using 9 mL $HNO_3$ and 200 µL HF and an ultraclave (MLS, Germany).

The elemental contents of the visually clear digests were determined using inductively coupled plasma - mass spectrometry (ICP-MS, Agilent 7500cx or 8900QQQ, Agilent, USA) or ICP-optical emission spectrometry (ICP-OES, SPECTRO Arcos, Germany) depending on the analyte concentration. National Institute of Standardization and Technology (NIST) standard reference material (SRM) 1643f was used for Cu, Zn, Al and Fe quality control (QC) of the respective ICP measurements.

Further, NIST SRM 2782 (industrial sludge) and NIST SRM 1633c (coal fly ash) were used to assess the recovery of Cu and Zn from comparable matrices during chemical digestion. Recovery from SRM 2782

was 89% for Cu and 92% for Zn. Recovery from SRM 1633c was 93% for Cu and 103% for Zn. Cu/Zn concentrations in sludge/ash were corrected for these recoveries.

A benchtop X-ray fluorescence (XEPOS+, SPECTRO Analytical Instruments GmbH, Germany) spectrometer was used to quantify the elemental contents of Cu and Zn in selected samples. For that purpose, 4.0 g of powdered sample was mixed with 0.9 g of wax (Cereox Licowax, Fluxana GmbH, Germany) and pressed into pellets. For QC, the previously mentioned reference materials were used. Recovery from SRM 2782 was 86% for Cu and 96% for Zn. Recovery from SRM 1633c was 104% for Cu and 110% for Zn.

For X-ray diffraction, 200 mg of (nano) powder were dispersed in 1 mL of ethanol and dried on a Si sample holder for X-ray powder diffraction (XRPD) analysis. A X'Pert$^3$ Powder X-ray diffractiometer (PANalytical, The Netherlands) was used to record spectra from 5° to 95° 2-Θ (Co-$K_\alpha$) with a step size of 0.017° and a dwell time of 1.7 s per step.

A Mettler-Toledo DSC1 STAR thermogravimetric analyzer (TGA) was used to determine the ash content of the sludge samples. 5 to 7 mg of the powdered sludge were transferred into a 70 µL alumina ($Al_2O_3$) crucible. The crucible was placed on the balance in the TGA and kept under oxidizing atmosphere (25 mL/min $O_2$ flow) while heating the sample to 900 °C using a 10 K/min heating rate. The balance was protected by a 25 mL/min $N_2$ flow. For the determination of the fraction of solids in the sludge ($X_{TS}$), an aliquot of the dried sludge stored in the lab was collected and kept at 105 °C in an oven until the mass remained constant. The respective mass loss was attributed to moisture acquired during the storage of the samples.

The bisulfide ($HS^-$) concentration in digested sludge samples was determined iodometrically.[20]

## 2.3 Nanoparticles

CuO-NP and ZnO-NP were purchased as powders (Sigma-Aldrich, Germany). The size of the primary particles as indicated by the manufacturer was < 50 nm. Based on X-ray powder diffraction (XRPD),

CuO-NP and ZnO-NP were present as tenorite and zincite, respectively (Figure S5). For particle size analysis, 100 mg/L CuO and ZnO-NP were dispersed in 0.2% of surfactant (Novachem C-SUR-100, Postnova Analytics GmbH, Germany). Novachem C-SUR-100 contains a mix of ionic and non-ionic detergents. Dynamic light scattering (NanoZS, Malvern Instruments, UK) analyses indicated average number based particle diameters of 146 ± 41 nm and 173 ± 59 nm with poly-dispersity indexes of 0.31 and 0.15 for CuO-NP and ZnO-NP, respectively. The zeta-potential was $-40.8 \pm 0.4$ mV and $-36.9 \pm 0.8$ mV, the pH was 8.2 and 8.4 of CuO-NP and ZnO-NP dispersions, respectively. The NP in the spiking dispersion were additionally characterized using transmission electron microscopy (TEM) (Hitachi HT7700, 100 kV). Bright-field (BF)-TEM images revealed that CuO-NP had a primary particle size of roughly 50 nm and formed aggregates of 100 to 200 nm in dispersion. Similarly, ZnO-NP with a primary particle size of 70 nm formed aggregates of 200 to 300 nm (Figure S3).

## 2.4 Sewage sludge and ash samples

For the comparison between pilot scale and full scale incineration, digested and dewatered sludge samples from three different WWTPs in Switzerland (WWTP Rhein, Basel, WWTP ProRheno, Basel, and WWTP Werdhoelzli, Zurich) were collected. For convenience, sludges are referred to by the labels A, B and C, respectively. In addition to the sludge samples, corresponding ash samples were collected from the full-scale incineration facilities and are referred to as A-af, B-af, C-af ('af' for 'ash, full scale'). The sludge was dried at 105 °C overnight. Between 0.5 – 1.0 kg of dried sludge were crushed into pieces of several mm to a few cm and combusted in the pilot FBR at 820 – 840 °C during 1 to 2 h. The resulting ash samples are referred to as A-ap, B-ap and C-ap ('ap' for 'ash, pilot scale'). For analytical measurements, aliquots of 5 g the sludge were freeze dried.

Digested sewage sludge for Cu/Zn spiking experiments was collected at a municipal WWTP (Winznau, Switzerland). This specific sludge was selected due its low Cu and Zn contents as revealed by a previous screening study on the metal contents of sewage sludge in Switzerland.[13] The sludge was separated into 5 batches of 35 L each. Two batches were spiked with CuO-NP/ZnO-NP (D-NP), two batches were spiked

with $CuSO_4$/$ZnSO_4$ dissolved in water (D-AQ) and one batch was used as a control (D). The following amounts of Cu/Zn were spiked to the sludge after dispersion in 300 mL of 0.02% Novachem C-SUR-100 (Postnova, Germany) and sonication for 10 min (concentrations in element spiked dispersion/solution): 1,084 mg of CuO-NP (2,876 mg Cu/L), 3,383 mg of $CuSO_4 \cdot 5\ H_2O$ (2,868 mg Cu/L), 2,500 mg of ZnO-NP (6,695 mg Zn/L) and 8,881 mg of $ZnSO_4 \cdot 8\ H_2O$ (6,731 mg Zn/L). After spiking, the sludge was kept under anaerobic, mesophilic conditions (35 °C and continuous stirring) for 24 h. Thereafter, the sludge was dewatered using a centrifuge (3200 rpm, 4500 g), and further processed as described above.

## 2.5 X-ray absorption spectroscopy (XAS)

Dry sludge and fly ash samples were powdered in a ball mill (MM400, Rentsch, Switzerland) at 17 Hz for 4 min. Subsequently, 50 mg of the milled sample (sludge or ash) were mixed with 4 mg of boron carbide (Alfa Aesar, USA) and 150 mg of cellulose (Sigma-Aldrich, Germany) in an agate mortar. Boron carbide as a hard material helped to further mill and thus to homogenize the ash powder and cellulose provided stability to the pellets. An aliquot of 80 mg from the mixture was pressed into a 7 mm diameter pellet for XAS measurements. XAS data were recorded at the K-edges of Cu and Zn including X-ray absorption near edge (XANES) and extended X-ray absorption fine structure (EXAFS) spectra. XAS experiments were conducted at the X10DA (SuperXAS) beamline at the Swiss Light Source (SLS) (PSI, Villigen, Switzerland). Samples were measured in fluorescence mode using a 5-element Si drift detector (SGX Sensortech, Buckinghamshire, UK) and references were measured in transmission mode. Selected spectra of reference materials were recorded at BM26A (Dutch-Belgian beamline, DUBBLE) at the European Synchrotron Radiation Facility (ESRF, Grenoble, France) and at the X05LA (micro-XAS) beamline at the SLS. Crystalline CuS (covellite), $CuSO_4$ (copper sulphate), CuO (tenorite), ZnS (sphalerite), ZnO (zincite), $ZnFe_2O_4$ (franklinite), $ZnAl_2O_4$ (gahnite) and $CuFe_2O_4$ (cuprospinel) [21] were prepared for analysis in transmission mode. CuS, $CuSO_4$, CuO, ZnS, and ZnO were purchased chemicals (all Sigma-Aldrich, Switzerland), $ZnFe_2O_4$ $ZnAl_2O_4$ (both obtained from Sieber & Sieber, Switzerland) were separated as individual crystals from a host rock, and $CuFe_2O_4$ was prepared via solid state synthesis (Section S3) [22]. The samples and standards were measured at 100 K (using a CryoJet, Oxford instruments,

UK) at SLS and 80 K (using a He cooled cryo stat) at ESRF. Cu- or Zn-foils were recorded simultaneously for energy calibration. $E_0$ was chosen based on the half height of the edge jump of the Cu/Zn-foil spectrum. Data treatment and linear combination fitting (LCF) were conducted using Athena [23], and for principle component analysis (PCA) and target testing (TT) SIXPack[24] was used.

## 2.6 Mass balance calculations

Mass balance calculations were established for total mass (sludge and ash) and for Cu/Zn recovered from sludge and ash samples. The mass balance for the total mass was:

$$m_{\text{sludge}} X_{\text{TS}} X_{\text{ash}} = m_{\text{fly}} + m_{\text{flt}} + m_{\text{bottom}} , \quad (1)$$

where $m_{\text{sludge}}$ was the mass of sludge (dried at 105 °C and stored in the lab) which was incinerated, $m_{\text{fly}}$, $m_{\text{bottom}}$, and $m_{\text{flt}}$ were the recovered masses of fly and bottom ash and the ash in the filter bag. $X_{\text{TS}}$ is the fraction of solids in the dried and stored sludge and obtained by drying the stored sludge at 105 °C and $X_{\text{ash}}$ represents the ash content of the sludge obtained by heating the sludge from 105 °C to 850 °C in the TGA (Section 2.2). The recovery of the ash content expressed as % is calculated according to equation 2:

$$\text{Recovery of ash content} = \frac{m_{\text{fly}} + m_{\text{flt}} + m_{Bottom}}{m_{\text{sludge}} X_{\text{TS}} X_{\text{ash}}} [\%]. \quad (2)$$

The mass balance based on the Cu/Zn concentration can be calculated using equation 3.

$$m_{\text{sludge}} c_{\text{sludge}} = \sum_{i=1}^{3} m_{\text{ash,i}} c_{\text{ash, i}} \quad (3)$$

The index $i$ refers to fly ash ($i = 1$), bottom ash ($i = 2$) and filter bag ash ($i = 3$). $m_{ash,i}$ and $c_{\text{ash, i}}$ refer to the mass of ash and the concentration of Cu/Zn of the respective ash type and $c_{\text{sludge}}$ refers to the concentration of Cu/Zn in the dried sludge. The recovery of Cu/Zn scaled by the recovery of the ash content and can be calculated according to equation 4:

$$\text{Recovery of Cu/Zn} = \frac{\sum_{i=1}^{3} m_{ash,i} c_{\text{ash, i}}}{m_{\text{sludge}} c_{\text{sludge}}} \times \frac{1}{\text{Recovery of ash content}} [\%]. \quad (4)$$

The mass of the ash collected in the filter bag was negligible and thus excluded from the mass balance calculations. Furthermore, enrichment factors (*EF*s) were calculated for the spiking experiments for Cu and Zn according to equation 5:

$$EF = \frac{c_{\text{fly}} * m_{\text{fly}} + c_{\text{bottom}} * m_{\text{bottom}}}{m_{\text{fly}} + m_{\text{bottom}}} \times \frac{1}{c_{\text{sludge}}}. \quad (5)$$

# 3 Results and Discussion

## 3.1 Total carbon, Cu and Zn concentrations in sludge and ash

**Total carbon concentrations (TC).** TC concentrations of A to C were 25, 26 and 34% (Table S1). Resulting fly ashes from the pilot FBR contained 3.2, 3.2 and 1.7 % TC (2.4% ± 0.8%), and corresponding fly ashes from full scale incineration facilities contained 0.2, 0.1 and 0.2 % TC (0.2% ± 0.1%). The digested sludge from the Cu/Zn spiking experiment (D, D-NP, D-AQ) contained 29.3 ± 0.4% (n = 5) TC. Corresponding fly and bottom ashes contained 1.6% ± 0.2% and 0.011% ± 0.003% TC, respectively.

TC concentrations in fly ashes from full scale incineration facilities were 1.5 to 3% lower compared to the fly ashes produced by the pilot FBR. However, due to longer residence time in the fluidized bed, TC concentrations in the bottom ashes were comparable to the TC concentrations in the fly ashes from the full scale facilities. Therefore, a shorter residence time of the fly ash in the fluidized bed and the freeboard of the pilot incinerator may have resulted in slightly higher TC concentrations in the pilot compared to the full-scale fly ash.

**Cu/Zn concentrations pilot– full-scale comparison.** Cu concentrations of the unspiked sludge samples collected from the three WWTPs (A, B, C) used for the comparison between pilot- and full- scale incineration were between 95 and 380 mg/kg and between 250 and 1100 mg/kg in the respective fly ashes (Figure 1 a and Table S1). The Zn concentrations in the sludge samples were between 530 and 940 mg/kg and 1250 and 3560 mg/kg in the corresponding fly ashes (Figure 1 d). Cu/Zn concentrations are based on ICP-MS and-OES measurements of clear digests. Results from XRF measurements were in good agreement with Zn concentrations measured by ICP-MS/OES (red X's, Figure 1 and Table S1).

Concentrations of Cu determined by XRF, however, were slightly lower than concentrations measured by ICP-MS/OES. This may be related to different Cu recoveries obtained for the NIST SRM 1633c (coal fly ash) samples and the sewage sludge ash samples, caused by the different types of matrices.

**Cu/Zn concentrations spiking experiments.** Cu concentration in sludge D was 391 ± 1 mg/kg and increased to 832 ± 1 mg/kg and 539 ± 4 mg/kg in D-ap fly ash and in the bottom ash, respectively (Figure 1 b). Cu concentrations in Cu spiked D-NP and D-AQ were 1244 ± 4 mg/kg and 1483 ± 38 mg/kg, respectively. The Cu concentrations in the corresponding fly ashes (D-NP-ap and D-AQ-ap) increased to 2735 ± 53 mg/kg and 3011.1 ± 53 mg/kg. Cu concentrations in the bottom ashes were 1481 ± 17 mg/kg and 2435 ± 95 mg/kg.

The Zn concentrations in D was 805.8 ± 39.9 mg/kg and increased to 2888 ± 30 mg/kg and 2706 ± 78 mg/kg in the corresponding fly- and bottom ash (Figure 1 e). Zn concentrations in Zn-spiked D-NP and D-AQ-were 6239 ± 1475 mg/kg and 5285 ± 298 mg/kg. The Zn concentrations in the corresponding fly ashes (D-NP-ap and D-AQ-ap) were 14382 ± 825 and 13588 ± 448 mg/kg. Zn concentrations in both bottom ashes were 10553 ± 328 mg/kg and 13144 ± 670 mg/kg.

## 3.2 Mass balances and Cu/Zn enrichment of the incineration experiments

In general, the mass recoveries were between 80% and 120%, and only for the sample D-AQ (Cu) the mass recovery was lower (59%) (Table S2). Thus, considering the complexity of the experiments, a satisfactory mass closure was obtained. Deviations from 100% recovery are likely caused by incomplete collection of the ash at the end of the experiment. Recoveries of Cu ranged from 47% to 91% with a mean and median of 69% and 65%, respectively (Table S2). Recoveries of Zn range from 65% to 114% with a mean and median of 92% and 91%, respectively. The fair closure of the mass balances and the low masses retained by the filter bags indicate that (i) all significant mass streams have been collected, (ii) the electrostatic filters efficiently retained the ash particles and (iii) Cu and Zn were mainly associated with the ash rather than volatilized during incineration.

Enrichment factors (*EFs*), calculated according to equation 5 are shown (Figure 1 c and f). Error bars were determined based on the propagation of uncertainty. Ideal *EFs* (1/ash content) equal to 2.48 (dashed lines Figure 1 c and f)). For the Cu and Zn spiking experiments conducted with the unspiked sludge (no addition of Cu/Zn), triplicate measurements were available, as sludge spiked with Zn-NP or $Zn_{(aq)}^{2+}$ can be considered as unspiked sludge regarding Cu (the same applies for Zn). *EFs* for Cu and Zn varied between 1.3 and 2.5 and 1.6 and 3.8. There was no consistent trend based on NP/AQ spiking suggesting that the Cu/Zn enrichment was independent of the form and concentration of Cu and Zn spiked to the digested sludge.

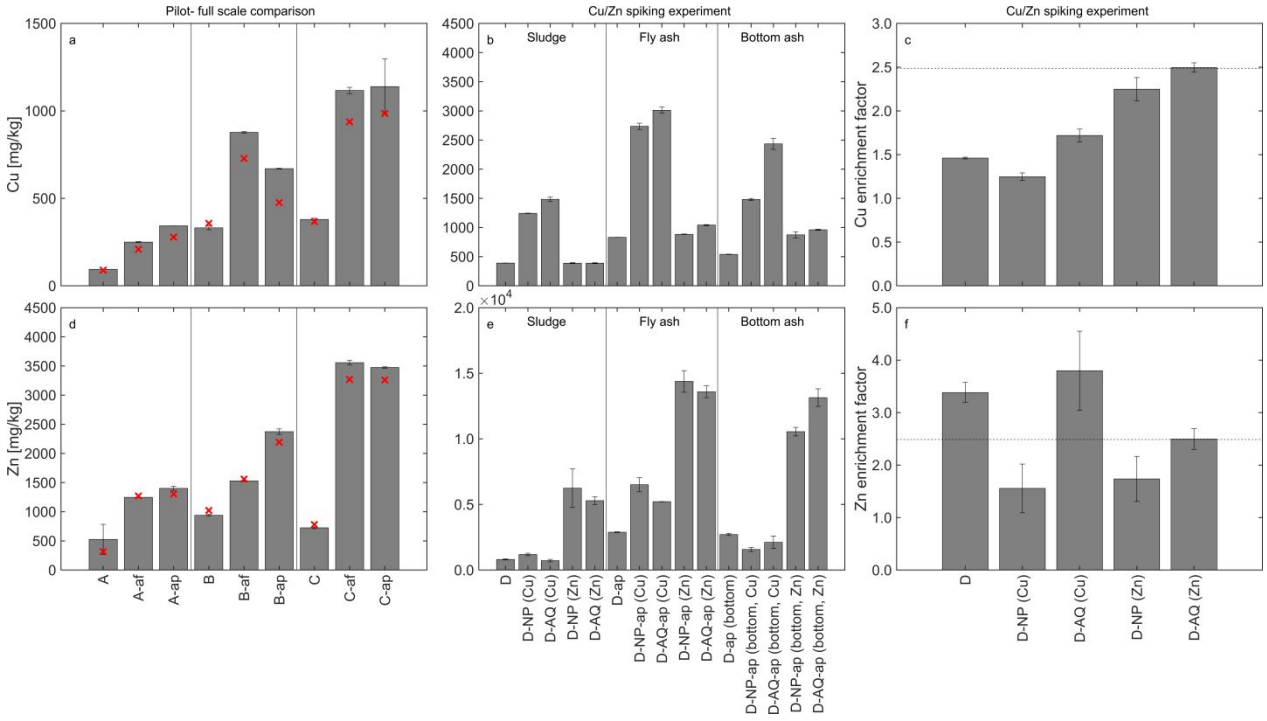


Figure 1: Cu concentrations in digested sludge samples and in ash samples from pilot and full-scale incinerators (a). Cu concentration in the spiked samples (b). Cu enrichment factors (EF), calculated from the spiking experiments (c). Standard deviations of EFs are determined according to Gaussian propagation of uncertainty (all in grey bars). Corresponding information for Zn are given in d to f. The red X's indicate the concentration determined by XRF. The dashed, horizontal bars in (c) and (f) indicate the ideal *EF* (2.49) corresponding to 1/ash content. Letters 'A' to 'D' refer to different sludge samples. The additions

252 'NP' or 'AQ' indicate that either CuO/ZnO-NP or $Cu^{2+}$(aq)/$Zn^{2+}$(aq) was spiked to the sludge. The
253 additions of 'af' and 'ap' refer to ash samples resulting from either a full scale incinerator or from the pilot
254 FBR.

## 255 3.3 Cu and Zn speciation in digested sludge and ash samples from pilot- and field
## 256 scale incinerators

257 We evaluated the Cu/Zn speciation in the digested sludge and assessed whether the ashes produced by the
258 pilot FBR showed comparable Cu /Zn speciation as the ash resulting from field scale incineration
259 facilities. We used principle component analysis (PCA) and target testing (TT) to Cu/Zn EXAFS spectra
260 to determine appropriate reference materials (Section S8). Linear combination reconstruction (LCR) is
261 performed to the respective XANES to evaluate the comparability between recorded EXAFS and XANES.

262 **Cu speciation.** XANES spectra of three digested sludge samples (A to C) exhibit a similar shape with a
263 distinct feature at 8986 eV (Figure 2 a, vertical line). After incineration in field and pilot FBRs, the shape
264 of the spectra changed considerably and the ash spectra showed more variability compared to the sludge
265 spectra (A-af to C-af and A-ap to C-ap). The spectra of B-af and C-af have a similar shape, but A-af
266 appeared different with more prominent oscillations expressed at 9002 eV which is also reflected in the
267 loadings of the first two principle components (PC), determined by PCA (Figure S10). The spectra of the
268 ashes derived from the pilot incinerator are very similar and, with the exception of A-ap, also very
269 comparable to the full-scale ashes.

270 The EXAFS spectra were evaluated by LCF to quantify the major spectral components describing the
271 sample spectra (Figure 2b). The spectra A to C were best described by $Cu_xS$ (amorphous), which
272 contributed between 70 and 85% to the total fractions returned by LCF (Figure 2 c). Minor fractions were
273 assigned to crystalline Cu-S phases (chalcopyrite, covellite) (total Cu-S between 84 - 92%) and Cu(II)
274 bound to oxygen (Cu(II)-O) (tenorite, copper sulphate, Cu(II)-acetate).

Through incineration, the speciation of Cu markedly changed as reflected by the XANES and EXAFS data of the digested sludge and the corresponding ashes (Figure 2a to c). After incineration roughly one third (28 to 37%) of the Cu species was described by Cu-S (amorphous $Cu_xS$, covellite, chalcopyrite) (Figure 2 c). The remaining fraction was best described by Cu(II)-O, with about 20 - 30% assigned to tenorite, 5 to 35% to $CuSO_4$, 5 to 40% to cuprospinel and up to 20% Cu-acetate for the full scale ash samples. The different reference spectra of oxygen coordinated Cu(II) compounds (Cu(II)-O) were included to account for minor variations in the Cu(II)-O bonding environments, but do not imply that these specific phases were present in the samples. The difference between A-af, A-ap and the other two ashes is reflected by a lower fraction of $CuSO_4$ and a correspondingly higher fraction of cuprospinel in the A-af sample. However, the sum of Cu(II)-O is almost identical in all ash samples.

LCR based on EXAFS LCF analyses generally described the XANES data well, indicating a good agreement between LCF results obtained from both XANES and EXAFS data (Figure 2 a). In general, the data showed that a substantial part of the sulfidized Cu present in the sludge was transformed into oxide-forms during incineration.

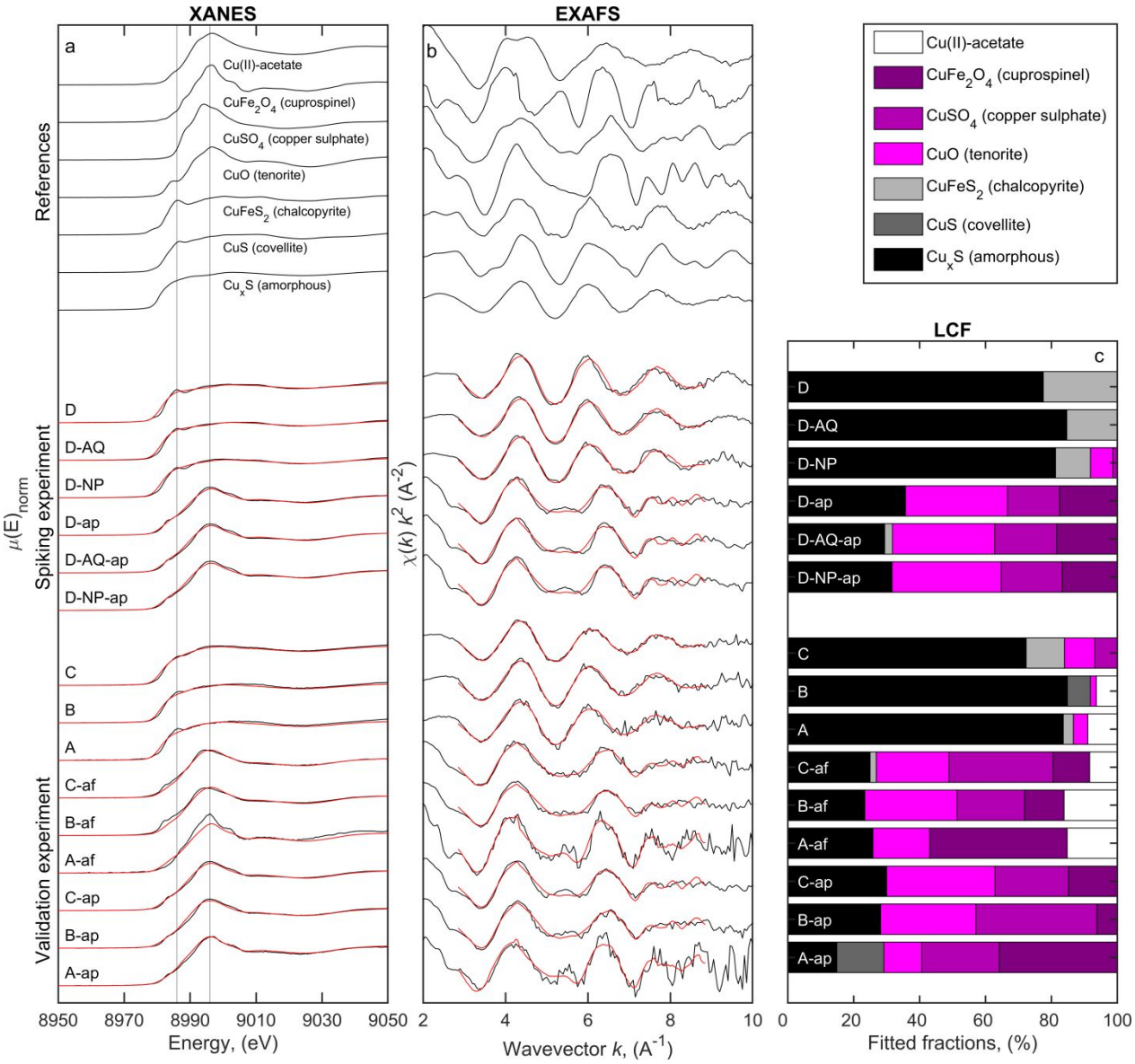


Figure 2: Cu K-edge XAS results. XANES of the references (upper part), samples from spiking experiment (middle part) and full-scale-pilot-scale comparison (lower part), indicated by black lines (a). Respective EXAFS spectra indicated by black lines are given in (b). The red lines indicate linear combination fit results to the EXAFS from 3 to 9 $A^{-1}$ (b). The respective fitted fractions are given in (c). The red lines in (a) indicate linear combination reconstructions of the fitted fractions reported in (c). Samples A – D represent digested sewage sludges, D-NP represents sludge spiked with CuO-NP, D-AQ spiked with dissolved $CuSO_4$. The addition "af" refers to ash obtained from a field scale FBR, the "ap" refers to the ash generated in the pilot FBR. The fractions displayed in (c) are listed in the SI (Table S10).

299

300 **Zn speciation.** XANES data of the three digested sludge samples A to C (Figure 3 a) appear very similar
301 and show the most prominent oscillation at 9664 eV (vertical line, Figure 3 a). This oscillation closely
302 matches the sphalerite reference spectrum, suggesting a very comparable and sulfide dominated chemical
303 speciation in all digested sludge samples, in agreement with other observations of the Zn speciation in
304 biosolids.[18-19] Since the XANES/EXAFS spectra of sphalerite are nearly identical to those of wurtzite
305 (ZnS),[25] the data do not allow to differentiate between these two host phases.

306 LCF analysis of the EXAFS spectra was performed from $k = 3 - 10\ \mathrm{A}^{-1}$. The resulting fractions for the
307 sludge spectra were dominated by sphalerite (50 to 70%) with variable fractions of a Zn-ferrihydite co-
308 precipitate. (Zn-Fh CPT) (20 to 45%) (Figure 3 b and c). Zincite only plays a minor role (< 10%) in fitting
309 the sludge spectra and might as well be related to artifacts caused by the varying quality of the spectra.

310 EXAFS shell fitting of the Zn spectrum of the Zn-Fh-CPT reference material suggested Zn to be
311 tetrahedrically coordinated to oxygen. Together with the bonding distance of 3.48 A to the second shell
312 (Fe) this suggests that Zn is incorporated in a weakly crystalline spinel like phase (Section S6).

313 The ash XANES spectra show more variability compared to the sludge spectra. A-af and A-ap exhibit four
314 intense oscillations at 9664, 9668, 9673 and 9687 eV (vertical lines in Figure 3 a). Three of these
315 oscillations (9664, 9673 and 9687 eV) are also observed in the reference spectra of $ZnAl_2O_4$ (gahnite), a
316 high temperature spinel phase, typically found in magmatic and metamorphic rocks in which Zn is
317 tetrahedrally coordinated with oxygen.[26] The feature at 9668 eV coincides with the most prominent
318 oscillation of the zincite reference spectrum. The spectra of all other ash samples, exhibit the same
319 oscillations, but less intense.

320 EXAFS LCF analyses of the ashes revealed a complete absence of the ZnS reference, indicating a more
321 complete chemical transformation of Zn compared to Cu (Figure 3 b). The ash spectra could mostly be

reproduced by a major fraction of Zn-Fh CPT (65 to > 90%) combined with variable fractions of gahnite up to 35%.

The fractions of Zn-Fh-CPT and gahnite determined by LCF in combination with the finding that franklinite ($ZnFe_2O_4$) was not a suitable reference (Section S8) suggest that Zn in the fly ash was dominantly tetrahedrally coordinated with O in (weakly crystalline) spinel-like structures, with variable formation of more crystalline Zn-Al (or similar, e.g. $Zn_nMg_{1-n}Al_2O_4$ [27]) spinel phases. This is in in agreement with previous observations where Zn was reported to be tetrahedrally coordinated to O,[28] possibly in a spinel-like structure [29] in coal fly ash. Zn in gahnite, in addition to octahedrally-coordinated Zn, has previously also been identified in thermally treated fly-ash from a municipal solid waste incinerator.[30]

LCR of the fitted fractions to XANES gave good results for sludges A to C, but matched less accurately the ash samples. Especially the XANES of A-af and A-ap were not well described by the LCR. XANES is more sensitive to the arrangement of the closest neighboring atoms compared to EXAFS which integrates information over a longer size range. Therefore, the different degrees of crystallinity of the gahnite and the Zn-Fh-CPT references resulted in different fractions obtained from LCF to XANES or EXAFS data.

Elevated fractions of gahnite coincided with a strong expression of the oscillations at 9664, 9668, 9673 and 9687 eV (A-af, A-ap and B-af, Figure 3 a). The highest fractions of gahnite were fitted to A-af and A-ap. The Al/Fe ratio in the corresponding sludge A was 0.49 (Table S1). In rare cases, $Al^{3+}$ is used to precipitate $PO_4^{3-}$ in WWTPs, leading to elevated Al concentrations in resulting sludges.[7] The Al/Fe-ratio of B and C were significantly lower (0.19 and 0.24, respectively), possibly explaining the lower fractions of gahnite returned by the LCF fits. However, the highest spinel fractions for Cu (cuprospinel, Figure 2 c) were equally observed in A-af and A-ap samples. Therefore, in addition to the Al/Fe-ratio also other sludge properties may be responsible for the high spinel fractions returned by LCF analyses of these ash spectra.

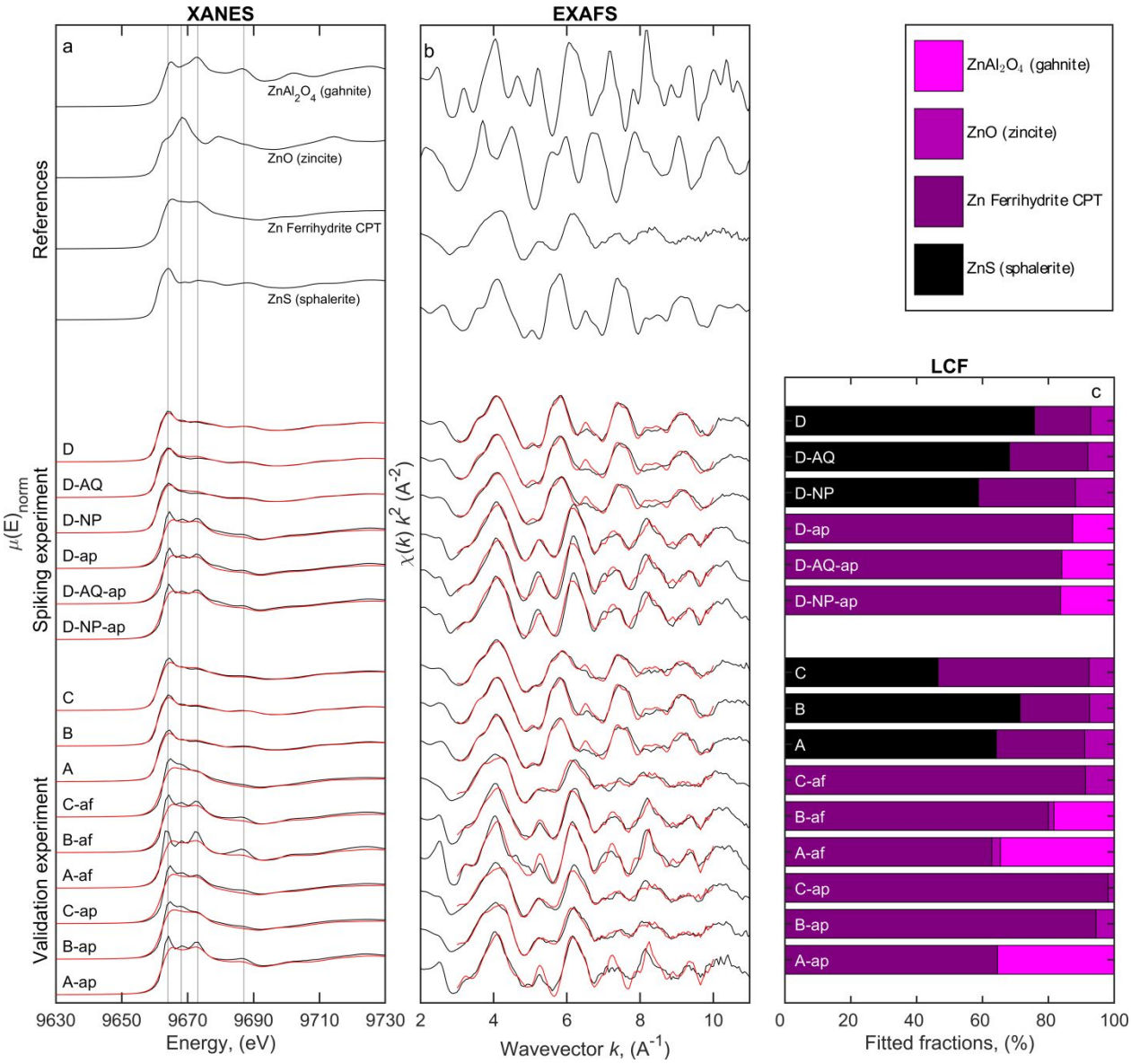


Figure 3: Zn K-edge XAS results. XANES of the references (upper part), samples from spiking experiment (middle part) and full-scale - pilot-scale comparison (lower part), indicated by black lines (a). Respective EXAFS spectra, indicated by black lines are given in (b). The red lines indicate linear combination fit results to the EXAFS from 3 to 10 A$^{-1}$ (b). The respective fitted fractions are given in (c). The red lines in (a) indicate linear combination reconstructions of the fitted fractions reported in (c). Samples A – D represent digested sewage sludges, D-NP represents sludge spiked with ZnO-NP, D-AQ spiked with dissolved $ZnSO_4$. The addition "af" refers to ash obtained from a field scale FBR, the "ap" refers to ash generated in the pilot FBR. The exact quantities displayed in (c) are listed in SI (Table S11).

## 3.4 Performance of the pilot FBR

Mass balance calculations conducted for total masses and Cu/Zn yielded a satisfactory mass closure for all experiments conducted on the pilot FBR. Lower values obtained for Cu compared to Zn recoveries are most likely explained by analytical issues related to the recovery of Cu. Approximately 95% of the total carbon was devolatilized during the incineration in the pilot FBR. The chemical speciation of Cu and Zn in digested sludge samples collected from different WWTP was very comparable and minor differences for example regarding the Cu speciation may be explained by different wastewater sources (e.g. industrial vs. municipal or type of phosphate precipitation). With the exception of A-af, also the chemical speciation of Cu/Zn observed in the ash samples from the full-scale facilities were very similar and almost indistinguishable from the respective ashes produced in the pilot FBR. Furthermore, the speciation of Cu/Zn in the bottom ash and in the fly ash produced in our incinerator was very comparable (Section S7). Incineration in the pilot FBR therefore resulted in comparable transformations as observed in field scale incinerators. Based on these finding, we conclude that relevant chemical transformations occurring during the incineration of sewage sludge can reliably be traced using the pilot FBR.

## 3.5 CuO and ZnO -nano particle transformation during sewage sludge digestion and incineration

XAS measurements were conducted to assess the chemical speciation of Cu/Zn in unspiked digested sludge, in sludge spiked with either CuO-NP/ZnO-NP or $Cu_{(aq)}^{2+}$/$Zn_{(aq)}^{2+}$ (D, D-NP and D-AQ) and in their corresponding ash samples (D-ap, D-NP-ap and D-AQ-ap).

**Cu transformation**. XANES of digested sludge samples (D, D-NP and D-AQ) exhibited comparable shapes (Figure 2 A). Minor differences included the oscillation observed at 8986 eV which was most prominently expressed in the spectra of the unspiked sludge (Figure 2 a). This oscillation is characteristic for Cu in crystalline reduced sulfur environments, here represented by covellite and chalcopyrite. Furthermore, a pre-edge feature can be observed in the spectrum of the unspiked sludge at 8979 eV, which is also present in the reference spectrum of chalcopyrite (Figure 2a). This pre-edge feature is absent in D-

NP and D-AQ and suggests larger fractions of Cu present as amorphous $Cu_xS$ as compared to crystalline copper sulfides.[31] Based on the kinetics of CuO-NP reacted with $HS^-$ eventually resulting in the complete formation of covellite after 3 hours [32], we reacted the spiked Cu over a period of 24 h in the digested sludge. This reaction time, however, may have been too short to allow establishing thermodynamic equilibrium between the Cu phases resulting in slight differences between the chemical speciation of Cu in D and D-NP/D-AQ (e.g. higher fraction of amorphous $Cu_xS$ phases in spiked sludges). Our results compare well with results reported by Gogos et al. [33] where CuO-NP reacted predominantly to an amorphous $Cu_xS$ in the presence of organic compounds. However, besides these minor differences there was a good agreement between the chemical speciation of Cu from the unspiked and the spiked sludge samples. Qualitative results from XANES analyses, thus suggest that Cu in digested sludge is dominantly present as sulfidic species, irrespective of the initial from of Cu ('native', nanoparticulate or dissolved).

LCFs were performed on the EXAFS spectra ($k = 3 - 9\ \mathrm{A}^{-1}$). For Cu in digested sludge, the available reference spectra adequately described the experimental spectra (Figure 2b). The spectra of D and D-AQ can be reconstructed by a combination of the spectral components representing amorphous $Cu_xS$ (77% and 85%) and chalcopyrite (23% and 15%), where the fraction of chalcopyrite is slightly larger for the spectrum of the unspiked sludge (Figure 2c). In the sludge, the formation of $CuFeS_2$ is thermodynamically favorable (Figure S14). However, initial $Cu_xS$ precipitation precedes the formation of other copper sulfides,[31] and thus, kinetic hindrance of the transformation of $Cu_xS$ precipitates into more crystalline Cu-Fe-S phases (covellite and chalcopyrite) may explain the lower share of $CuFeS_2$, in both spiked sludge samples compared to the unspiked sludge sample, which had more time to equilibrate. In the case of sludge spiked with CuO-NP, a minor fraction (7%) of CuO was returned by the LCF analysis which was accompanied by a slightly lower fraction of chalcopyrite compared to the spectra from the other two sludge samples. CuO – $Cu_xS$ core-shell structures as reported in a recent study [33] may protect the CuO cores over extended periods of time and may thus explain the minor contribution of CuO returned by the LCF analyses of the EXAFS spectra of Cu-NP spiked sludge samples. Alternatively, formation of CuO-NP agglomerates may also slow down the transformation kinetics.

XANES LCR of the sludge sample spectra based on EXAFS LCF were generally in good agreement with the XANES spectra, although a slightly mismatch can be observed at around 8986 eV (Figure 2 a). This mismatch likely reflects the preference of XANES LCF for more crystalline reference spectra compared to EXAFS LCF as discussed in Section 3.3.

Although minor differences in the chemical speciation were observed between the NP spiked (D-NP) and the other two sludge samples (D and D-AQ), the spectra resulting from the corresponding ashes appear almost identical. Solely, the oscillation observed at 8982 eV, which is characteristic for crystalline Cu-S phases, is slightly stronger expressed in D-ap compared to D-NP-ap and D-AQ-ap (Figure 2a). In all ash samples, roughly 35% of the total Cu was represented by spectral components characteristic for Cu-S, and the remaining 65% were shared between spectral components of Cu(II)-O (tenorite (31 – 33%), cuprospinel (17 – 18%), and copper sulphate (16 – 19%)) (Figure 2 b and c). Therefore, the differences in the speciation of Cu between the sludge samples which were revealed by LCF disappeared through the incineration process.

**Zn transformation**. XANES spectra of sludge samples (D, D-AQ and D-NP) all exhibit a similar shape (Figure 3 a). The oscillations in D are expressed slightly stronger compared to the other two spectra (D-AQ and D-NP), which is an indication that the Zn in the spiked sludge samples did not yet match the speciation of the Zn in the unspiked sample. EXAFS LCF ($k = 3 - 10\ \mathrm{A}^{-1}$) suggests that the sludge spectra can generally be described by spectral components of sphalerite (60 - 75%) and Zn-Fh CPT (15 - 30%) (Figure 3 b and c). EXAFS LCF to D and D-AQ returned comparable fractions of zincite ( $\approx 7\%$). However, the ZnO-NP spiked sample showed a slightly higher fraction of ZnO (11%), possibly reflecting the formation of ZnS – ZnO core shell structures resulting in a retardation of the transformation of ZnO to ZnS. In analogy to the observations made for the transformation of Cu and the corresponding discussions, also the transformation kinetics of Zn may be reduced in the presence of organic compounds.[34] Our results are in agreement with the rapid sulfidation of $Zn_{(aq)}^{2+}$ and the retarded sulfidation of ZnO-NP spiked to anaerobically digested sewage sludge.[19]

All ash spectra exhibit a very comparable shape (Figure 3a). LCF to D-ap was best described by 87% Zn-Fh-CPT and 13% gahnite. Both, D-NP-ap and D-AQ-ap were best described by 84% Zn-Fh-CPT and 16% gahnite. Therefore, the incineration process also unifies the Zn speciation.

Using transmission electron microscopy, an additional attempt was made to identify potential differences in nanoscale element distribution between ash samples from differently spiked sludges (D-NP-ap, D-AQ-ap) (Figure S13). Although, nanoscale Zn-bearding precipitates were discovered in ash from Zn-NP spiked sludge (D-NP-ap, ZnO), similar structures were also observed in ash from the incineration of $ZnSO_4$-spiked sludge (D-AQ-ap, $ZnSO_4$). Furthermore, nanoscale Cu-rich phases were also observed in ash from ZnO-spiked sludge, illustrating that also 'background' Cu already present in the sludge can occur in nanoscale Cu-precipitates after incineration. In general, however, nanoscale precipitates were only very rarely observed, which prevents to draw any statistically sound conclusions from these observations. We therefore can neither exclude nor confirm that morphological differences at the nanoscale are preserved in ash resulting from the incineration of sludge spiked with Cu/Zn in dissolved vs. nanoparticulate forms.

Recently, a series of studies described the transformation of ENPs in managed waste facilities including sewer systems [2, 35], WWTPs[3, 36], anaerobic digestion[19, 37], sewage sludge and municipal waste incineration.[38-42] Consistent results were reported from wastewater and sludge treatment systems (anaerobic digestion), whereas to some extent contradictory observations were reported from incineration studies. Auffan et al.,[43] reported that $CeO_2$-NP remained unaffected during the combustion process, whereas Gogos et al.[38] found that d°=°4 nm primary $CeO_2$-NP were entirely sequestered into mineral phases newly formed during anaerobic digestion (≈°30%) followed by fluidized bed incineration (100%). However, most of the discrepancies observed between different studies are probably related to an oversimplification of the experimental setup. In general, these studies, in agreement with the finding reported from this study, consistently indicate that the ENPs are very reactive and can hardly escape form urban environments in their pristine forms.

## 3.6 Implications for risk assessment and exposure modeling

Both Cu and Zn are classified as chalcophile metals and are thus expected to dominantly coordinate with inorganic and organic reduced sulfur in wastewater systems. High $HS^{--}$ contents (6.5 to 8 mM $HS^-$ in our experiments) typically observed during anaerobic digestion thus resulted in the formation of Cu- and Zn-sulfides. Kinetic hindrance, possibly through the formation of metal-oxide – metal-sulfide core-shell structures or the formation of agglomerates, may have resulted in slightly higher fractions of Cu/Zn bound to O in samples spiked with CuO/ZnO-NP compared to sludge spiked with $Cu_{(aq)}^{2+}$/$Zn_{(aq)}^{2+}$ and unspiked sludge. Considering typical retention times in full-scale anaerobic digesters in the order of 30 d, which are considerably longer than the reaction times of 24 h evaluated in this study, the speciation of spiked nanoparticulate and dissolved Cu and Zn as well as of Cu and Zn from other sources corresponding to the Cu and Zn that was already present in the unspiked sludge, are expected to converge over longer times under field conditions. Incineration of the digested sludge resulted in the (partial) sequestration of Cu and Zn into (possibly nanoparticulate) oxide mineral structures. Furthermore, the chemical speciation of Cu and Zn in ash samples, resulting from spiked (D-NP, D-AQ) and unspiked sludge samples were indistinguishable. The study exemplifies the complex reactions of engineered CuO and ZnO NP in various managed waste facilities resulting in an almost identical chemical speciation as observed for Cu and Zn entering managed waste facilities as 'background' Cu and Zn, possibly as dissolved species, nanoscale colloids or micrometer-sized particles. Although the transformation of the ENPs (and metals added in other forms) may still result in the formation of new nano-particulate phases, such incidental particles will be classified as by-products and differ from the original ENPs. The transient nature of ENP in managed waste facilities must, therefore, be considered in mass flow analyses and risk / exposure assessments.

**Supporting Information.** Contains 31 pages, 14 figures and 11 tables on the pilot fluidized bed reactor, ENP characterization, the cuprospinel synthesis, detailed results of the sample characterization and mass balances, statistical results of the PCA/TT, the EXAFS LCF and equilibrium calculations.

# 4 References


1. Lazareva, A.; Keller, A. A., Estimating Potential Life Cycle Releases of Engineered Nanomaterials from Wastewater Treatment Plants. *ACS Sustainable Chemistry & Engineering* **2014,** *2* (7), 1656-1665.
2. Kaegi, R.; Voegelin, A.; Ort, C.; Sinnet, B.; Thalmann, B.; Krismer, J.; Hagendorfer, H.; Elumelu, M.; Mueller, E., Fate and transformation of silver nanoparticles in urban wastewater systems. *Water Research* **2013,** *47* (12), 3866-3877.
3. Kaegi, R.; Voegelin, A.; Sinnet, B.; Zuleeg, S.; Hagendorfer, H.; Burkhardt, M.; Siegrist, H., Behavior of Metallic Silver Nanoparticles in a Pilot Wastewater Treatment Plant. *Environmental Science & Technology* **2011,** *45* (9), 3902-3908.
4. Westerhoff, P.; Song, G.; Hristovski, K.; Kiser, M. A., Occurrence and removal of titanium at full scale wastewater treatment plants: implications for TiO2 nanomaterials. *Journal of Environmental Monitoring* **2011,** *13* (5), 1195-1203.
5. Fytili, D.; Zabaniotou, A., Utilization of sewage sludge in EU application of old and new methods—A review. *Renewable and Sustainable Energy Reviews* **2008,** *12* (1), 116-140.
6. Kelessidis, A.; Stasinakis, A. S., Comparative study of the methods used for treatment and final disposal of sewage sludge in European countries. *Waste Management* **2012,** *32* (6), 1186-1195.
7. Tchobanoglous, G., Stensel, H.D., Tsuchihashi, R. and Burton, F.L.,, *Wastewater engineering: treatment and resource recovery*. McGraw-Hill Education: New York, NY, USA: 2013.
8. EUROSTAT, Sewage sludge production and disposal: Sludge production - total. *Water statistics on national level* **2016**.
9. EUROSTAT, Sewage sludge production and disposal: Sludge disposal - incineration. *Water statistics on national level* **2016**.
10. Werther, J.; Ogada, T., Sewage sludge combustion. *Progress in Energy and Combustion Science* **1999,** *25* (1), 55-116.
11. Laube, A.; Vonplon, A., Klärschlammentsorgung in der Schweiz, Mengen- und Kapazitätserhebung. *BUWAL* **2004**.
12. Simoni, M.; Kuhn, E. P.; Morf, L. S.; Kuendig, R.; Adam, F., Urban mining as a contribution to the resource strategy of the Canton of Zurich. *Waste Management* **2015,** *45*, 10-21.
13. Vriens, B.; Voegelin, A.; Hug, S. J.; Kaegi, R.; Winkel, L. H. E.; Buser, A. M.; Berg, M., Quantification of Element Fluxes in Wastewaters: A Nationwide Survey in Switzerland. *Environmental Science & Technology* **2017,** *51* (19), 10943-10953.
14. Monser, L.; Adhoum, N., Modified activated carbon for the removal of copper, zinc, chromium and cyanide from wastewater. *Separation and Purification Technology* **2002,** *26* (2), 137-146.
15. Ju-Nam, Y.; Lead, J. R., Manufactured nanoparticles: An overview of their chemistry, interactions and potential environmental implications. *Science of The Total Environment* **2008,** *400* (1), 396-414.
16. Llorens, A.; Lloret, E.; Picouet, P. A.; Trbojevich, R.; Fernandez, A., Metallic-based micro and nanocomposites in food contact materials and active food packaging. *Trends in Food Science & Technology* **2012,** *24* (1), 19-29.
17. Wiechmann, B.; Claudia, D.; Christian, K.; Simone, B.; Ines, V.; Andrea, R., Sewage Sludge Management in Germany. *Umweltbundesamt Deutschland, January* **2015**.
18. Donner, E.; Howard, D. L.; Jonge, M. D. d.; Paterson, D.; Cheah, M. H.; Naidu, R.; Lombi, E., X-ray Absorption and Micro X-ray Fluorescence Spectroscopy Investigation of Copper and Zinc Speciation in Biosolids. *Environmental Science & Technology* **2011,** *45* (17), 7249-7257.
19. Lombi, E.; Donner, E.; Tavakkoli, E.; Turney, T. W.; Naidu, R.; Miller, B. W.; Scheckel, K. G., Fate of Zinc Oxide Nanoparticles during Anaerobic Digestion of Wastewater and Post-Treatment Processing of Sewage Sludge. *Environmental Science & Technology* **2012,** *46* (16), 9089-9096.
20. A. Eaton, L. C., R. Rice, A. Greenberg and M. Franson, Standard methods for the examination of water and wastewater. *American Public Health Association (APHA): Washington, DC, USA* **2005**.

21. Prince, E.; Treuting, R. G., The structure of tetragonal copper ferrite. *Acta Crystallographica* **1956,** *9* (12), 1025-1028.
22. Tasca, J. E.; Quincoces, C. E.; Lavat, A.; Alvarez, A. M.; González, M. G., Preparation and characterization of CuFe2O4 bulk catalysts. *Ceramics International* **2011,** *37* (3), 803-812.
23. Ravel, B.; Newville, M., ATHENA, ARTEMIS, HEPHAESTUS: data analysis for X-ray absorption spectroscopy using IFEFFIT. *Journal of Synchrotron Radiation* **2005,** *12* (4), 537-541.
24. Webb, S. M., SIXpack: a graphical user interface for XAS analysis using IFEFFIT. *Physica Scripta* **2005,** *2005* (T115), 1011.
25. Dana, J. D.; Dana, E. S.; Palache, C.; Berman, H.; Frondel, C., *The System of Mineralogy of James Dwight Dana and Edward Salisbury Dana... 1837-1892: Elements, Sulfides, Sulfosalts, Oxides*. Wiley: 1944.
26. Deer, W. A.; Zussman, J., *Rock-forming minerals: Sheet silicates*. Wiley: 1962; Vol. 3.
27. Singh, V. K.; Sinha, R. K., Low temperature synthesis of spinel (MgAl2O4). *Materials Letters* **1997,** *31* (3-6), 281-285.
28. Luo, Y.; Giammar, D. E.; Huhmann, B. L.; Catalano, J. G., Speciation of Selenium, Arsenic, and Zinc in Class C Fly Ash. *Energy & Fuels* **2011,** *25* (7), 2980-2987.
29. Shoji, T.; Huggins, F. E.; Huffman, G. P.; Linak, W. P.; Miller, C. A., XAFS Spectroscopy Analysis of Selected Elements in Fine Particulate Matter Derived from Coal Combustion. *Energy & Fuels* **2002,** *16* (2), 325-329.
30. Struis, R. P. W. J.; Ludwig, C.; Lutz, H.; Scheidegger, A. M., Speciation of Zinc in Municipal Solid Waste Incineration Fly Ash after Heat Treatment: An X-ray Absorption Spectroscopy Study. *Environmental Science & Technology* **2004,** *38* (13), 3760-3767.
31. Pattrick, R. A. D.; Mosselmans, J. F. W.; Charnock, J. M.; England, K. E. R.; Helz, G. R.; Garner, C. D.; Vaughan, D. J., The structure of amorphous copper sulfide precipitates: An X-ray absorption study. *Geochimica et Cosmochimica Acta* **1997,** *61* (10), 2023-2036.
32. Gogos, A.; Thalmann, B.; Voegelin, A.; Kaegi, R., Sulfidation kinetics of copper oxide nanoparticles. *Environmental Science: Nano* **2017,** *4* (8), 1733-1741.
33. Gogos, A.; Voegelin, A.; Kägi, R., Influence of organic compounds on the sulfidation of copper oxide nanoparticles. *Environmental Science: Nano* **2018**.
34. Ma, R.; Levard, C.; Michel, F. M.; Brown, G. E.; Lowry, G. V., Sulfidation Mechanism for Zinc Oxide Nanoparticles and the Effect of Sulfidation on Their Solubility. *Environmental Science & Technology* **2013,** *47* (6), 2527-2534.
35. Brunetti, G.; Donner, E.; Laera, G.; Sekine, R.; Scheckel, K. G.; Khaksar, M.; Vasilev, K.; De Mastro, G.; Lombi, E., Fate of zinc and silver engineered nanoparticles in sewerage networks. *Water Research* **2015,** *77*, 72-84.
36. Ma, R.; Levard, C.; Judy, J. D.; Unrine, J. M.; Durenkamp, M.; Martin, B.; Jefferson, B.; Lowry, G. V., Fate of Zinc Oxide and Silver Nanoparticles in a Pilot Wastewater Treatment Plant and in Processed Biosolids. *Environmental Science & Technology* **2014,** *48* (1), 104-112.
37. Doolette, C. L.; McLaughlin, M. J.; Kirby, J. K.; Batstone, D. J.; Harris, H. H.; Ge, H.; Cornelis, G., Transformation of PVP coated silver nanoparticles in a simulated wastewater treatment process and the effect on microbial communities. *Chemistry Central Journal* **2013,** *7* (1), 46.
38. Gogos, A.; Wielinski, J.; Voegelin, A.; Emerich, H.; Kaegi, R., Transformation of cerium dioxide nanoparticles during sewage sludge incineration. *Environmental Science: Nano* **2019,** *6* (6), 1765-1776.
39. Impellitteri, C. A.; Harmon, S.; Silva, R. G.; Miller, B. W.; Scheckel, K. G.; Luxton, T. P.; Schupp, D.; Panguluri, S., Transformation of silver nanoparticles in fresh, aged, and incinerated biosolids. *Water research* **2013,** *47* (12), 3878-3886.
40. Walser, T.; Limbach, L. K.; Brogioli, R.; Erismann, E.; Flamigni, L.; Hattendorf, B.; Juchli, M.; Krumeich, F.; Ludwig, C.; Prikopsky, K.; Rossier, M.; Saner, D.; Sigg, A.; Hellweg, S.; Gunther, D.; Stark, W.

J., Persistence of engineered nanoparticles in a municipal solid-waste incineration plant. *Nat Nano* **2012,** *7* (8), 520-524.
41. Meier, C.; Voegelin, A.; Pradas del Real, A.; Sarret, G.; Mueller, C. R.; Kaegi, R., Transformation of Silver Nanoparticles in Sewage Sludge during Incineration. *Environmental Science & Technology* **2016,** *50* (7), 3503-3510.
42. Vejerano, E. P.; Leon, E. C.; Holder, A. L.; Marr, L. C., Characterization of particle emissions and fate of nanomaterials during incineration. *Environmental Science: Nano* **2014,** *1* (2), 133-143.
43. Auffan, M.; Tella, M.; Liu, W.; Pariat, A.; Cabié, M.; Borschneck, D.; Angeletti, B.; Landrot, G.; Mouneyrac, C.; Giambérini, L.; Rose, J., Structural and physical–chemical behavior of a CeO2 nanoparticle based diesel additive during combustion and environmental release. *Environmental Science: Nano* **2017,** *4* (10), 1974-1980.

# 5 Acknowledgments

The authors thank Brian Sinnet, Marco Kipf and Matthias Philipp for their support in the laboratory and during the incineration experiments. We acknowledge funding from the Swiss National Science Foundation (grant 5221.01038.001) and from the European Union's Horizon 2020 research and innovation program (NanoFASE) under grant agreement No. 646002. Further, we acknowledge support from the staffs at the SuperXAS (X10DA) and micro-XAS (X05LA) Beamlines at the Swiss Light Source (SLS) and the staff at the Dutch-Belgium Beamline (BM26A) at the European Synchrotron Radiation Facility (ESRF). We also like to acknowledge the ETH Zürich Microscopy Center (ScopeM) for providing access to their electron microscopes. We thank Mr. Grob and Mr. Aareeger at WWTP Winznau, Ms. Weber from WWTP ProRheno, Mr. Hurschler from WWTP Rhein and Mr. Nussbaumer from WWTP Werdhoelzli for providing digested sewage sludge and/or sewage sludge ash.